Published in final edited form as:
Nat Struct Mol Biol. 2015 December ; 22(12): 991–998. doi:10.1038/nsmb.3120.

The role of lipids in mechanosensation

Christos Pliotas[1], **A. Caroline E. Dahl**[2], **Tim Rasmussen**[3], **Kozhinjampara R Mahendran**[4], **Terry K. Smith**[1], **Phedra Marius**[1], **Joseph Gault**[4], **Thandiwe Banda**[3], **Akiko Rasmussen**[3], **Samantha Miller**[3], **Carol V. Robinson**[4], **Hagan Bayley**[4], **Mark S. P. Sansom**[2], **Ian R. Booth**[3,5], and **James H Naismith**[1,6]

[1]Biomedical Sciences Research Complex, University of St Andrews, St Andrews KY16 9ST, UK

[2]Department of Biochemistry, University of Oxford, Oxford OX1 3QU, UK

[3]Institute of Medical Sciences, University of Aberdeen, Aberdeen AB25 2ZD, UK

[4]Department of Chemistry, University of Oxford, Oxford OX1 3TA, UK

[5]Division of Biology and Biological Engineering, California Institute of Technology, Pasadena, California, 91125, USA

[6]State Key Lab of Biotherapy, Sichuan University, China

Abstract

The ability of proteins to sense membrane tension is pervasive in biology. A higher resolution structure of *E. coli* MscS, the channel of small conductance, identifies alkyl chains inside pockets formed by the transmembrane helices (TMs). Purified MscS contains *E. coli* lipids and fluorescence quenching demonstrates that phospholipid acyl chains exchange between bilayer and TM pockets. Molecular dynamics and biophysical analyses show that the volume of the pockets and thus the number of lipid acyl chain within them decreases upon channel opening. Phospholipids with one acyl chain per head group (*lyso*lipids) displace normal phospholipids (two acyl chains) from MscS pockets and trigger channel opening. We propose the extent of acyl chain interdigitation in these pockets determines the conformation of MscS. Where interdigitation is perturbed by increased membrane tension or by *lyso*lipids, the closed state becomes unstable and the channel gates.

Correspondence to: James H Naismith.

Author Contributions

CP purified and spin labeled MscS for lipid analysis, single molecule analysis, crystallisation, obtained and analysed the new crystal structure, participated in the single molecule and lipid analysis experiments. TR purified MscS for, carried out and analysed the fluorescence studies including synthesis of brominated lipids. ACED wrote the MD analysis software, performed and analysed the simulations. KRM performed and analysed single molecule experiments. AR made mutants of MscS and performed osmotic downshock assays. TB assisted in fluorescence experiments. TKS performed lipidomic mass spectrometry. CVR & JG carried out native mass spectrometry. PM performed TLC experiments. SM, HB, MSPS, IRB and JHN conceived and supervised the study.

All authors wrote, reviewed and approved the paper, and the authors disclose no conflicts of interest.

CP, ACED, TR & KRM share first authorship

Accession Codes

PDB 5aji

Europe PMC Funders Author Manuscripts

Keywords

Lipids; Ion channels; MscS; pressure sensing; lateral tension; turgor pressure

Introduction

Organisms use lipid bilayers, impermeable to ions and polar molecules, to compartmentalize. The exchange of molecules with the outside world occurs in a controlled manner *via* channels and transporters. In general transporters respond to the presence of their substrates and energy, whereas channels respond to specific stimuli. Mechanosensitive channels gate in response to changes in the tension in the membrane bilayer. Mechanosensors are found in bacteria, archaea[1,2] and in eukaryotes[3], where they fulfill a variety of essential roles. The role of the human piezo channels in cardiovascular disease has recently attracted attention[4]. However, the best studied mechanosensitive channels are MscS and MscL from *E. coli*[5-7], which open in response to increased turgor pressure to save the cell from rupture during osmotic shock[8-10].

In addition to an open (conducting) and a closed (non-conducting) state, sub-conducting (partly open) states have been observed for MscS[11-14]. An open state can be generated *in vitro* by addition of *lyso*-phosphatidylcholine (LPC 18:1) to liposomes or spheroplasts[15,16] or by application of pressure in a patch pipette[17]. Mechanosensitive channels, in particular MscS, have become influential models in probing pressure-sensing[2,7,18]. An open[19] and a closed[20] structure of the MscS in conjunction with site-directed mutagenesis has led to a model of how the protein changes during gating[19].

MscS has four transmembrane helices (TM1, 2, 3a and 3b, Fig 1A,B), TM1-2 pack together in an antiparallel arrangement approximately perpendicular to the plane of the membrane and TM3a lines the central pore (Fig 1A,B). TM3b, predicted to be located at the interface between lipids and cytosol is approximately parallel to the membrane. Rotational symmetry results in the cytoplasmic domains of MscS forming a large enclosed space with portals through which solutes pass. In the closed state[20] the TM3a helices are tightly packed creating a hydrophobic seal[12,21]. Upon gating TM3a helices move akin to a camera iris opening the pore whilst TM1-2 rotate 50° around the pore[19]. ‘Voids’ exist between TM3a,b and TM1-2[19,20]. The volume of voids differs between the open and closed structures[19,20]. MscS structures lacking ‘voids’ have been generated by continuous wave EPR[16] and computation[22]. Pulsed EPR studies on the MscS protein in both detergent solution[23] and lipid bilayers[24] as well as crystal structures of MscS solubilized in different detergents[25] and from different organisms[25,26] all possess ‘voids’ between the TMs. Such voids are seen in other membrane proteins[27,28].

Molecular insights into how lateral tension within the lipid bilayer is sensed have been elusive but must account for the role of the lipids[2,29,30]. Our understanding has been profoundly changed by the observation that eukaryotic K^+ ion channels are modulated by membrane tension[31,32]. Regulation of ion channels by membrane tension may be general and one of nature’s oldest mechanisms[31,33,34]. MscS (and MscL) in a bilayer are sufficient for tension sensing[35,36]. In the study of the human TRAAK K^+ channel, whose function is

modulated by membrane tension[32], changes in membrane tension were transmitted by changes in lipid protein interactions[5,37].

We set out to probe how pressure is sensed by MscS. We develop a model that has reversible lipid interdigitation in the protein voids as the central feature. We suggest the model may have broader validity.

Results

Lipids pack the 'voids' in MscS

MscS D67C single-cysteine mutant was covalently modified as described[38] to give MscS D67R1 (R1 denotes MTSSL cysteine adduct). A MscS D67R1 crystal[23] diffracted to 3.0 Å resolution (Table 1, Supplementary Fig. 1). The protein structure is essentially identical to the 3.45 Å A106V open structure[19]. We have located a few additional residues and spin labels which match the measured PELDOR distances[23] (Supplementary Fig. 1A, B). Difference (Fo-Fc) electron density at the transmembrane helices was fitted as alkyl chains (Fig 1B, Supplementary Fig. 1C) but was not sufficiently unambiguous to differentiate between lipid and detergent[39]. Two alkyl chains penetrate into the 'pocket' formed by the arrangement of TM1-TM2 and TM3b in the heptamer whilst the third chain packs against TM3b (Fig 1A). This is the first experimental evidence that the 'voids' in MscS are 'pockets' that contain lipids or lipid-like molecules.

After detergent extraction and purification of the native MscS heptamer up to five putative lipids bound to MscS heptamer in the gas phase were resolved in non-denaturing mass spectrometry[40] (Fig 2A). A series of peaks were observed with mass differences between 620 to 790 Da, ruling out DDM (510 Da) or LDAO (230 Da) adducts; detergents used in sample preparation. The lowest mass species is a lipid adduct of protein, not the protein alone (seen for other membrane proteins[40]). The mass range of small molecule adducts is consistent with the two major types of *E. coli* phospholipid (PL), phosphatidylethanolamine (PE) and phosphatidylglycerol (PG), but not cardiolipin (CL).

Two independent preparations of DDM-purified MscS D67R1 had their lipids extracted and analyzed by mass spectrometry (Fig 2B). ES-MS and subsequent MS fragmentation detected seven lipid species, six were assigned (Fig 2B). PG ionizes more readily than PE (Fig 2B) preventing quantitative analysis, however, changes in the relative counts of species between samples are indicative of changes in the relative proportions of the phospholipids. PG 30:1 and in particular PE 14:0/14:0 and PE 16:1/14:0 were enriched relative to their natural abundance in *E. coli* [41]. The differences in phospholipid composition in the protein sample were not a feature of *E. coli*, were independent of detergent, but specific to MscS (Supplementary Fig. 2A-D).

Lipid extract from purified MscS was examined in thin layer chromatography (TLC) were stained with primuline to differentiate lipid from detergent and with ninhydrin to identify PE (ninhydrin does not stain PG or CL phospholipids) (Fig 2C). The plates show PE is indeed the predominant phospholipid. A previous SEC-ICP-MS study [42] estimated 2.6 to 3 unidentified phospholipids per MscS monomer. Based on TLC we estimate around 0.5 PE

molecules per monomer (consistent with non-denaturing MS analysis, Fig 2A). A protein sample that had been in detergent for several months and subjected to multiple freeze-thaw cycles showed a lower PE: protein ratio (Fig 2C, Supplementary Table 1). We suggest that the precise lipid content may reflect differences in the purification and storage procedure.

The lipids exchange between the pockets and bilayer

We performed multi-scale molecular dynamics (MD) simulations (1 μs coarse grain (CG-MD) and 100 ns atomistic (AT-MD), 5 replicates of each) on both the closed[20] and open structures (D67R1 mutated *in silico* to native) in a 4:1 POPE:POPG lipid bilayer model. The protein structure was restrained to prevent collapse of the pockets and distortion of TMs. In all simulations lipids migrate to fill the TM pockets with more lipids in the lower than upper half of the pocket (Fig 3A, B and Supplementary Fig. 3A, B). Strong local membrane curvature is observed around MscS in both states (Fig 3A, B) consistent with the proposal that the local membrane environment around MscS is highly distorted[43]. The distortion of the membrane bilayer around MscS (Figure 3A,B, Supplementary movie 1 and 2) highlights the limitations of a simple geometric representation of the bilayer as a flat sheet and illustrates the importance of characterizing the exact disposition of the lipids in order to understand tension transmission. Previous simulations identified a smaller degree of curvature[44] but these simulations were shorter (< 10 ns) and used a simpler POPC lipid bilayer. The N-terminal 24 residues of MscS, which are disordered, are excluded from models but may play some role. The tapered shape of MscS is manifested in the different protein cross sectional areas at periplasmic and cytoplasmic membranes (Fig 3A,B, Fig 1 and Supplementary Fig. 1D). The volume of the transmembrane pore in the open structure has increased due to the outward movement of the TM3a helices towards to TM1-2 (Fig 1C)[19] which has concomitantly compressed the inter-helical pockets (Fig 1C, Supplementary Fig. 1D).

CG-MD shows that as MscS opens the lipid content of the pocket decreases by approximately one lipid per pocket (Fig 3A, B, C and Supplementary Fig. 3A, B), the loss occurs between TM2 and TM3a (Supplementary Fig. 3D). The pockets (upper and lower regions) are more accessible to lipids of the cytosolic membrane leaflet (Fig 3A, B and Supplementary Fig. 3A, B). The lipids in the pockets are mobile and in continuous contact with the bulk membrane bilayer (Supporting movie 1 and 2), in particular the cytosolic leaflet (Fig 3A, B, C).

The simulations suggest that one lipid contact (per subunit) persists in the lower part of the pocket (Fig 3C). In the open state, these lipids are almost exclusively PE and overlap with alkyl chains in the crystal structure (Supplementary Fig. 3C). Protein proximity to these PE phospholipids remains essentially constant during the final 50 ns of AT-MD in agreement with CG-MD findings, consistent with the detection of PE phospholipids (Fig 2A, B, C). AT-MD shows that the zwitterionic headgroups of these phospholipids are coordinated primarily to charged residues on the loop that connects TM1-2 (Supplementary Fig. 3Fi). In the closed structure, TM3a helices are tightly packed and there is no lipid penetration of the pore (Supplementary Fig. 3Fii,iii) whereas in the open structure, the PE alkyl chains run parallel

to the TM3b helix and terminate by contacting L105 and L109 (the pore-sealing residues) by penetrating between adjacent TM3a helices; linking the bilayer through TM1-2 to TM3a.

Single Trp mutants were introduced into a tryptophan-free mutant of MscS, W16Y W240F W251F (MscS YFF) previously shown to be stable and functional, albeit with a reduced pressure sensitivity in patch clamp analysis[45]. A103W, V107W, and L111W on TM3a and L115W, A119W and L123W on TM3b were chosen as they line the pockets (Fig 1A, 3D). Except L115W which was unstable and eliminated from analysis, the mutants were functional (Supplementary Fig. 4A, B). M47W, on the surface of TM1 (lipid exposed), Q203W and native W240 on the cytosolic domain (no lipid contact) and L105W on TM3a (faces into pore, away from the pockets and thus lipids) were chosen as controls. MscS mutant channels were reconstituted by dilution[46,47] into lipid bilayers at a molar ratio of 100:1 (lipid:MscS monomer), with either non-brominated fatty acid chains, 1,2-dioleoyl-*sn*-glycero-3-phosphocholine (DOPC), or lipids that were brominated in the middle of the fatty acid chains, 1,2-di-(9,10-dibromo)stearoyl-*sn*-glycero-3-phosphocholine (BrPC) or small membrane patches in which BrPC forms bilayers with similar properties to DOPC[48,49].

When incubated with brominated lipids strong quenching was observed for the residues that face into the pockets (Fig 3D, E, Supplementary Table 2). The strongest quenching was observed with A119W but A103W and V107W also exhibited strong quenching (Fig 3E); these result indicate that the tryptophan is close the Br atom on the lipid. L123W, which lies closer to the periphery of TM3b, exhibited weak quenching possibly because it is close to the phospholipid head group region and consequently far from the Br atoms at the 9,10 positions of BrPC. Similarly, the less strongly quenching observed with the positive control M47W on TM1 (Fig 3E and Supplementary Table 2) may be explained by its proximity to lipid head groups as M47W. The three negative controls L105W, Q203W and W240 exhibited very weak or no quenching.

DOPC is not the natural lipid context for *E. coli* MscS, but has been used successfully[36,50]. L111W, A119W and L123W were retested in 4:1 PE:PG (*E. coli* like lipid composition) and yielded essentially the same results (Fig 3F). These data demonstrate that the cavities predicted from crystal structures permit exchange of phospholipids.

MscS is controlled by changes in protein lipid interactions

MscS opened with LPC 18:1 had a reported a single-channel conductance of 1 ± 0.2 nS (200 mM KCl, 90 mM $MgCl_2$, 10 mM $CaCl_2$, 10 mM HEPES)[16], similar to that obtained when trans-bilayer pressure differences were used to open[8,36]. LPC has been proposed to work by increasing leaflet curvature, mimicking the patch clamp pressure induced opening[15,16]. We reconstituted A119W and M47W MscS into DOPC and then added brominated LPC 18:1 to a final concentration of 33% (mole LPC: mole DOPC). Blue native gel analysis showed the MscS heptamer remained intact (Supplementary Fig. 4B). Comparison of spectra obtained before and after addition of LPC indicated quenching (Fig 4A). Dequenching was observed when both mutants were reconstituted into BrPC and non-brominated LPC added (Fig 4A). Thus LPC exchanges reversibly with lipids in the pockets. As DDM-solubilised MscS incubated with LPC 14:0 partially dissociates (Supplementary Fig. 4C) gel filtration was used to select heptameric protein. Mass spectrometric analysis of the lipid extract from the

heptameric fractions of MscS shows that LPC 14:0 remains associated with protein and has displaced the *E. coli* PE lipids (Fig 4B, Supplementary Fig. 4C,D,E).

There are no reports of MscS reconstituted into 1,2-diphytanoyl-sn-glycero-3-phosphocholine (DPhPC) planar lipid bilayers possibly because this system offers no simple way to establish a pressure gradient. However the planar bilayer technique offers defined access to each side of the membrane for additives (e.g. *lyso*phospholipids). In the absence of LPC, spontaneous currents were seen after reconstitution of MscS into the planar lipid bilayer; 70 % stable opening (Supplementary Fig. 5A), 30 % fast flickering (Supplementary Fig. 5B). The Unitary Conductance, G, was 1.2 ± 0.1 nS, (n = 25; Supplementary Fig. 5A, B), identical (within error) to that reported for MscS in patch clamp analyses[14,36,50-52]. Spontaneous openings were observed when MscS was reconstituted into liposomes[50]. Physical chemistry considerations favor the large cytoplasmic domain remaining on the *cis* side. Current-Voltage (I-V) curves obtained with the MscS reconstituted in a planar lipid bilayer showed the same rectification at negative potential (Supplementary Fig. 5C) as was observed where the orientation of channel was known (embedded in patches of the inner membrane)[36,50,52]. These data establish the validity of planar lipid bilayer system to probe MscS.

Lyso-PC 18:1 (3 μM) added to the *cis* compartment (cytoplasmic leaflet) activated MscS and yielded a unitary conductance of G = 0.8 ± 0.2 nS (n = 25) (Fig 4C); the openings are clearly distinguishable from the spontaneously opened channel. Around 20 % of openings are multiple sub-conducting states and short flickering events, while 80 % were free of flickering (n = 25) for 15 to 20 minutes (until bilayer ruptured, an effect presumably of LPC). Stable opening was observed after LPC 18:1 addition to the bath with inside-out patches of MscS[16] (equivalent to *cis* side). Addition of LPC 18:1 (final concentration 3 μM) to the *trans* compartment (periplasmic leaflet) opened MscS with the same conductivity as from the *cis* side (G = 0.8 ± 0.2 nS, n = 25), but with frequent closures (Fig 4D). LPC 14:0 (10 μM) added to the *cis* compartment gave similar results as LPC 18:1 but with stability of 30 to 45 min (Fig 4E). Over these longer traces multiple open channels were observed (Supplementary Fig. 5D). The addition of LPC 14:0 to the *trans* compartment resulted in channel opening (G = 0.8 ± 0.2 nS) with frequent gating (of variable duration) not sustained opening (Fig 4F). The statistically significant lower conductance with LPC 18:1 and LPC 14:0 (G = 0.8 ± 0.2 nS) compared to spontaneous opening (G =1.2 ± 0.1 ns) indicates that, at least in this system, LPC creates a sub (not fully) conducting state. D67C behaved as native in both planar lipid bilayers (Fig 5C) and in downshock assays[23]. D67R1 exhibited different behavior in planar lipid bilayers with no spontaneous opening and fluctuating and inconsistent behavior upon addition of LPC 14:0. MTSSL added to *E. coli* expressing D67C MscS (following a published approach[53]), results in native behavior in downshock assay (Supplementary Fig. 4F) suggesting the modified protein remains functional and that the spin label particularly effects LPC gating.

Discussion

A model for pressure sensing by MscS

The arrangement of the TM helices MscS creates pockets open to lipid bilayer (Fig 1A, 3A,B)[19,20,25,26]. The pockets are wedge shaped; the wider end at inner leaflet and the 'sharp and narrow end' in the outer leaflet. The TM1-2 helices create large hydrophilic grooves that span the bilayer. Truly empty pockets between the TM1-2 helices and TM3a-b are incompatible with a stable structure[22,44] and waters are unlikely to fill hydrophobic pockets. Doubts exist therefore on the validity of crystallography as means to explore MscS function. Pulsed EPR of MscS, both in detergent solution and reconstituted into bilayers, has supported the the presence of pockets[23,24]. We have shown specific phospholipids remain associated with MscS (Fig 2A,B,C). A 3.0 Å crystal structure and MD show that phospholipid (or lipid-like) molecules fill these pockets (Fig 1 and 3A,B). The profile of the pockets suggested that lipids most easily gain access from the cytoplasmic face and this is observed in the MD simulations (Fig 3A,B, Supplementary Fig. 3A, B and Supporting movie 1, 2). The role of the disordered residues (1-26) in these interactions is unknown; an important caveat to these results. That acyl chains fill hydrophobic grooves or pockets in membrane proteins is well known[54] and fluorescence quenching confirms that lipids exchange with lipids in the pockets (Fig 3E,F). MD calculations also show lipids in pockets to be dynamic, both within each state and in differences between states (Fig 3A,B,C and Supplementary Fig. 3A,B,D).

The fitting of a two state Boltzmann model to the observed plot of tension against open probability of MscS embedded in liposomes was used to derive a gating free energy of 29 kJ mol^{-1} and a change in cross-sectional area of 8.4 ± 0.4 nm^2 [36]. The structural data however gives cross sectional area change of 3 nm^2 and this results in a poor fit to the experimental tension data (Supplementary discussion & Supplementary Fig. 7). A second approach used protein cross sectional area at the midpoint, change in protein shape and the second derivative of pressure profile to derive an equation for MscL gating[55]. When parameters from the structural analysis of MscS are put into this formula the open structure is calculated to be more stable by 60 to 70 $KJmol^{-1}$ (Supplementary discussion), a result that we think unrealistic. These approaches, rooted in sound physical principles, assume that protein-lipid and lipid-lipid interactions do not change in response to pressure. We propose that, for MscS, the energy that arises from changes in lipid partition between the pockets and the bilayer is a previously missing component of tension sensing models.

The composition of the annular membrane and the specific interactions of lipids with MscS are known to be key to transmission of the mechanical stimulus[33,56]. Structural transitions of MscS upon gating[19,20] showed that the pockets are radically altered. Reliably estimating the change in volumes of the pockets is non trivial. Using 2.5 Å probe determines that upon opening each pocket is reduced by approximately 1200 $Å^3$; modifying the probe radii gave different results, but consistently showed a reduction in pocket volume. The loss of one lipid with two acyl chains was observed upon gating in molecular dynamics simulations (Fig 3C).

We propose that the conformational state of MscS is determined by the availability of lipids to fill the pocket; the closed structure, with larger pockets, needs at least one more

phospholipid molecule per monomer than the open state to be stable (Fig 3A, B). Biophysical measurements have established that lateral tension, not pressure *per se*, is the trigger for opening MscS[36,57]. Lateral tension exerts a 'pull' on lipid acyl chains inside the protein pockets (which are in exchange with the bilayer), as tension increases the equilibrium position of lipid molecules favors the bilayer not the pockets. This re-organisation of the lipids within and around the protein destabilises the closed structure. MscS gates to the open form with smaller pockets that need less lipid (Fig 5A); when the tension decreases the process reverses. (An equivalent formulation is at low tension lipids enter into pockets favoring the closed form, whereas at higher tension the reduction in lipids in the pockets allows the protein to adopt the open state.) This '*lipid moves first*' model is consistent with the exchange of lipids that we observed. Our model is the energy from re-organization of the acyl chains (i.e. between pockets and bilayer) (Fig 5A) is central to MscS tension sensing.

We do not favor a '*protein moves first*' model as it would require strongly bound lipids as force transducers at the mobile elements of MscS (TM1,2,3a). MD and biophysics showed the phospholipids to be in exchange (not tightly bound). Further a distinguishing features of MscS gating, the rotational motion of TM1-2[19], does not fit with lipids pulling the protein laterally.

LPC, a conical lipid, had been proposed to operate by changing curvature in one leaflet mimicking the curvature of patch clamping[58]. This proposal means that insertion on opposite (wrong) side of a bilayer would lead to bilayer curvature in the 'wrong' sense; that is curvature opposite to patch clamping[58]. The curvature model of LPC action predicts that LPC will only open the channel when added to the side of MscS where curvature mimics patch clamping. We observe that LPC14:0 open MscS with the same conductivity irrespective of side of addition; inconsistent with a curvature mechanism. LPC has recently been suggested to directly create tension in the bilayer[50] consistent with addition from either leaflet. However, we observe that an LPC opened structure has statistically significant lower conductance (Fig 4 C,D,E,F) than that opened by pressure[36] or that occurs spontaneously (Supplementary Fig. 5A, B); in short LPC creates a sub-conducting state.

The packing of the headgroups around the protein circumference[54] limits the number of acyl chains that could intercalate into the pockets (Fig 3A,B). However, *lyso*lipids, with one (not two) acyl chain per headgroup will, we suggest, be unable to stabilize the closed structure as efficiently as a normal phospholipid (Fig 5B). We propose this causes the sub-conducting state observed in single channel experiments (Figure 4,C,D,E,F). LPC can displace phospholipids from the pockets (Fig 4A,B) a requirement for this model of LPC action. Stable openings were observed when LPC is added at the cytoplasmic side, but opening with frequent closures were observed when LPC 18:1 (even more so LPC 14:0) was introduced from the periplasmic side (Fig 4D,F). Our biophysical data showing exchange of LPC with phospholipids (Figure 4A) cannot identify whether exchange occurs exclusively from the cytoplasmic face or from both faces. While MD calculations of bilayers with LPC added were beyond the scope of this paper, the origin of lipids in the pockets is primarily the cytoplasmic bilayer leaflet (Fig 3A,B and Supplementary Fig. 3A,B). Taken together we hypothesize that LPC will interact with the pockets most effectively from the cytoplasmic

face (Fig 5B) and this underpins the difference in behavior depending on the side of LPC addition. The gating of MscS by LPC is thus a special case of our general model in which it is lipid interdigitation that controls the channel's behavior. Lipid-induced changes in structure have been seen in pore forming toxins where host lipids activate the toxin[59].

Conclusion

Eukaryotic channels are now known to be modulated by pressure[7,31,32]. The sensitivity of TRAAK channel to membrane tension was shown to result from movement of a specific lipid in and out of a binding site in the TM helices[37]. In TRAAK there is a significant change in the cross sectional area of the protein but lipid re-organisation was noted a component of the TRAAK gating energy. In our model it is the lipid re-organisation (lipids shifting between interacting with protein via the pockets and with the bulk lipid of the bilayer phase) that changes the relative stabilities of these conformational states that in turn controls mechanosensation. We do not identify a specific key binding site as was seen in TRAAK[37]. It has been proposed that many mechanosensitive channels are activated by introduction of *lyso*lipids (or equivalents) and that other sensory channels, with ostensibly different gating signals, may share this property[34,60]. We predict that where different conformational states of a membrane protein differ in their capacity for sequestering phospholipids, changes in membrane tension or introduction of *lyso*lipids will modify (alongside other factors) the transition between the states.

Online Methods

Materials and Methods

Material—n-Dodecyl-β-D-maltopyranoside (DDM) and n-decyl-β-D-maltopyranoside (DM) anagrade were obtained from Anatrace Inc or Glycon (Germany). Isopropyl-β-D-thiogalactoside (IPTG) was obtained from Formedium and (*tris*(2-carboxyethyl)phosphine (TCEP) from Thermo Scientific Ltd. The *S*-(2,2,5,5-tetramethyl-2,5-dihydro-1H-pyrrol-3-yl)methyl methanesulfonothioate (MTSSL) spin label was obtained from Toronto Research chemicals, Toronto. Phospholipids, *E. coli* Polar Extract, PC, PE, PG, LPC 18:1 and LPC (14:0) were purchased from Avanti Polar Lipids. All other chemicals unless otherwise stated were obtained from Sigma. Mutants were generated with the Stratagene QuickChange™ protocol as described previously[12,19].

Biophysics

Purification and crystallization: MscS D67R1 single-cysteine spin-labeled mutant was expressed, purified, spin labeled and crystallized as reported previously[23]. The extent of spin labeling efficiency was quantified by using a fluorescence method described previously[38]. Briefly, the protein was concentrated by using Vivaspin concentrators (www.sartorius.com) with a 100 kDa cut-off, to 9-13 mg mL^{-1} in 0.05% DDM, 50 mM sodium phosphate, pH 7.5, and 300 mM NaCl. Crystals of MscS D67R1 grew to a full size of 0.3 mm × 0.1 mm × 0.1 mm, in two days. The best crystals (visual inspection) were obtained by using 0.07 M Nacitrate, pH 4.5, 0.07 M NaCl, 23% v/v PEG 400, as precipitant. Prior to data collection, crystals were transferred into a solution containing 0.07 M sodium citrate, pH 4.5, 0.07 M

Europe PMC Funders Author Manuscripts

NaCl and 30% v/v PEG 400. Data for MscS D67R1 were collected at 100 K on a single crystal on ID14-4 at the European Synchrotron Radiation Facility (ESRF) (Grenoble, France) and indexed, integrated and merged by using MOSFLM / SCALA[61] as implemented in CCP4[62] (Table 1). The resolution of the data used in refinement were determined following the procedure of Diederichs and Karplus [63,64] as it is implemented in the PDB REDO server[65]. This method has been shown to give more accurate models despite using weak data that are normally excluded by resolution cutoffs based on R-merge or I/σI criteria. Data and structure deposited with code 5aji. Pocket volumes were measured with with the CASTp server[66]

LPC treatment of purified MscS: *Lyso*-PC 14|:0 was dissolved in 0.05% DDM, 50 mM sodium phosphate, pH 7.5, and 300 mM NaCl and added to 30% molar ratio (LPC 14:0 / WT MscS monomer) purified in the same buffer WT MscS in an eppendorf tube. The tube was placed on the rocker at RT for 5 min and subsequently sonicated for another 5 min, for further incubation. The MscS containing tube and LPC 14:0 was kept on ice for a couple of minutes. The last three steps were repeated two more times. The sample was subjected to gel filtration (Superpose 6 column, GE healthcare) and run in a buffer containing 0.05% DDM, 50 mM sodium phosphate, pH 7.5, and 300 mM NaCl, without LPC 14:0.

The fractions of the peak corresponding to the heptamer of WT MscS were collected and concentrated using 100kDa cut off filters and then subjected to further lipid analysis.

Pore volume determination: The software Pore-Walker[67] was used for the determination of the pore diameter for MscS D67R1 and closed (2OAU) structures. For D67R1, the spin label was removed and the residue set back to native before analysis. In this calculation, only residues that were well resolved in both structures were taken into account and were aligned to the C-terminal end at residue 278, forming a total length pore axis of around 105 Å (e.g. a total number of 35 steps with each step being 3Å long). Pore disc surfaces were calculated for each step and subsequently integrated along the full length of the pore axis, resulting in the determination of the total pore volume using OriginPro 8.0.

Lipid volume determination: Lipid volumes were calculated for both truncated and full lipids from existing x-ray structures in the PDB database (Supplementary Table 3). Lipids with PE and PG headgroups were included in our analysis, because only these lipid-types were detected in the *E. coli* expression strain (Supplementary Fig. 2A). Volume calculations were made with Molspace (http://www.compbiochem.org/Software/molspace/Home.html) a plug-in of the VMD software routine[68].

Quenching of tryptophan fluorescence: Purification of the MscS tryptophan mutants followed in general the protocol established earlier[42,45]. Membranes were solubilised by incubation for 1 h at 4°C in 0.9% DDM (Glycon, Germany) containing 50 mM sodium phosphate, pH 7.5, 300 mM NaCl, 10% glycerol, 50 mM imidazole, 0.2 mM phenylmethylsulfonylfuoride (PMSF, Sigma). Aggregates were removed by centrifugation at 3000g for 10 min and filtration using 0.2 μm syringe filter. MscS was then bound through its C-terminal His_6-tag to a pre-packed 0.5 mL nickel-nitrilotriacetic (Ni-NTA) agarose column (Sigma) and washed with 20 mL of washing buffer (50 mM sodium phosphate, pH 7.5,

containing 0.05% DDM, 300 mM NaCl, 10% glycerol and 50 mM imidazole). After storage overnight at 4°C, MscS was eluted with elution buffer (washing buffer containing 300 mM imidazole). Peak fractions were separated on a Superdex 200 10/300 GL size exclusion column (GE Healthcare) at 0.5 mL min^{-1} using a buffer containing 0.03% DDM, 50 mM sodium phosphate, pH 7.5, 150 mM NaCl. All mutants studied here purified as heptamers as judged by the size exclusion chromatogram and proved to be functional *in vivo* as assessed by osmotic downshock assays after induction with IPTG[69].

Quenching experiments of tryptophan fluorescence were performed as described[46]. 1,2-dioleoyl-*sn*-glycero-3-phosphocholine (DOPC; Avanti, Alabaster) was brominated by the stepwise addition of bromine (Sigma) to a solution of the lipid in chloroform cooled on ice until a faint yellow colour of unreacted bromine persisted. Bromination of 1,2-dioleoyl-*sn*-glycero-3-phosphoethanolamine (DOPE; Avanti, Alabaster) and 1,2-dioleoyl-*sn*-glycero-3-phosphoglycerol (DOPG; Avanti, Alabaster) was performed by the same method. After a further 30 min, chloroform was removed under a nitrogen stream followed by several rounds of dissolving and evaporation. The brominated lipid 1,2-di-(9,10-dibromo)stearoyl-*sn*-glycero-3-phosphocholine (BrPC) was kept for several hours in a desiccator, dissolved again in chloroform and stored at −20 °C until further use. Bromination of DOPC was confirmed by NMR and mass spectrometry (Supplementary Fig. 6). Films of lipids were formed in thin-walled glass tubes by drying the desired amount of DOPC or BrPC as chloroform solutions under a nitrogen stream. The remaining chloroform was completely removed by keeping the glass tubes under vacuum at 4°C in a desiccator overnight. 2 μmol of DOPC or BrPC were then suspended under a nitrogen atmosphere in 1.6 mL of buffer A containing 40 mM HEPES, pH 7.2, 100 mM KCl, 1 mM EGTA, and 15 mM sodium cholate by warming the tube for 20 s in warm water, vortexing for 5 min, and subjecting to ultrasonication for 10 min (Fisher scientific, model FB15046). MscS (1.27 nmol, determined by UV/Vis spectroscopy using an extinction coefficient of ε_{280nm}(MscS 1W) = 15.9 $mM^{-1}cm^{-1}$) was added to lipid solution (100 μL, 127 nmol lipids) and incubated for 15 min at room temperature. MscS and lipids (25 μL) were added to measuring buffer B (600 μL, as buffer A but without sodium cholate) in a 4×4 mm stirred quartz cell (Hellma, Germany). Measurements were performed after 5 min incubation (in the case of L105W after 15 min incubation because of slower equilibration) in a FLS920 fluorescence spectrometer (Edinburgh Instruments) with excitation at 295 nm and emission from 300 to 420 nm at 20°C. Excitation and emission slits were set to 3 nm and 7 nm, respectively, and polarizers at 90° and 0°, respectively[70]. The emission at 340 nm was used for analysis of quenching. This wavelength was chosen to avoid some effect of tyrosine fluorescence at low wavelengths (300-320 nm), strong scattering at low wavelengths (<305 nm), Raman scattering (327 nm), and higher noise at longer wavelengths caused by low tryptophan fluorescence intensities. The emission at 340 nm was corrected with samples containing lipids but no MscS. Fractional quenching was calculated from the fluorescence intensities at 340 nm as $FrQ=(F_0-F)/F_0$, where F_0 is the intensity for the sample containing 100% non-brominated lipids and F for 100% brominated lipids. Experiments with mixtures of 80% DOPE and 20% DOPG or their brominated forms were performed in the same way than with DOPC or BrPC. Brominated LPC (made as described for BrPC) or LPC were added (0.33 mol/mol of total lipid) to A119W MscS samples reconstituted in DOPC in the same

way as described above. MscS was reconstituted in BrPC following the same procedure as described for DOPC.

The function of the studied mutant forms of MscS was assessed by an osmotic downshock assay as described earlier[69]. The MscS constructs in the vector pTrc99A with an added C-terminal His-tag were transformed into the *Escherichia coli* strain MJF612[71] and an overnight culture was grown in LB medium supplemented with 25 μg/ml ampicillin at 37°C. The next day the culture was diluted 100 times to fresh medium and grown to an OD_{650nm} of 0.4. The cultures were then diluted 10 times into a LB medium with an additional 0.5 M NaCl and grown until an OD_{650nm} of 0.3. For each sample two of these cultures were grown where one of them was supplemented with 0.3 mM IPTG at an OD_{650nm} of 0.2. All samples were diluted 20 times into LB medium (shock) and into LB + 0.5 M NaCl (control). After serial dilutions into similar media, samples were grown on plates and colonies were counted the next day. Survival was quantified as counted colonies for shock samples relative to control samples.

Analysis of lipid content

Native Mass Spectrometry: Native mass spectra were acquired using a Q-TOF 2 instrument (Micromass) equipped with a Z-spray source and modified to allow the transmission of high molecular weight species[72]. Aliquots of MScS in dodecyl-β-D-maltopyranoside (DDM) were buffer exchanged using biospin-6 columns (Bio-Rad) first into 200 mM Ammonium acetate 0.02% DDM and then into 200 mM ammonium acetate 0.05% lauryldimethylamine-oxide and electrosprayed from gold coated nano-spray capillaries in the positive ion mode[73]. Optimised instrument parameters include collision cell pressure capillary voltage 1500 V, sample cone 200 V, extractor 10 V, backing pressure 8.79×10^{-3} mbar, collision cell pressure 0.31 MPa, collision energy 150 V and argon was used as the collision gas. All spectra were calibrated externally using a solution of cesium iodide (25 mg/mL). Spectra were acquired for around 100 scans then processed (summed then smoothed) using MassLynx V4.1 (Waters). Masses were calculated using software developed in house.

ES-MS and ES-MS-MS lipidomic analysis: Lipid removal from purified recombinant proteins was achieved by 3 successive vigorous extractions with ethanol to fully denature the proteins (final 90% v/v)[74]. The pooled extracts were dried with nitrogen gas in a glass vial and re-extracted by using a modified Bligh and Dyer method[75]. To obtain a complete lipid extract from *E. coli* cells, cells were washed with PBS, suspended in PBS (100 μL), transferred to a glass tube containing chloroform:methanol (1:2, 375 μL) and vortexed. The sample was agitated vigorously for a further 10-15 min, made biphasic by the addition of $CHCl_3$ (125 μL) and water (125 μL), vortexed again and centrifuged at 1000g at room temperature for 5 min. The lower organic phase was transferred to a new glass vial, dried under nitrogen and stored at 4°C.

Lipid extracts were dissolved in chloroform : methanol (1:2, 15 μL) and acetonitrile : isopropanol : water (6:7:2, 15 μL) and analyzed with a Absceix 4000 QTrap, a triple quadrupole mass spectrometer equipped with a nanoelectrospray source. The samples were

delivered using a Nanomate interface in direct infusion mode (~125 nL min^{-1}). The extracts were analysed in both positive and negative ion modes using a capillary voltage of 1.25 kV. MS-MS scanning (daughter, precursor and neutral loss scans) were performed using nitrogen as the collision gas with collision energies between 35-90 V. Each spectrum encompasses at least 50 repetitive scans.

Tandem mass spectra (MS-MS) were obtained with collision energies as follows; 35-65V, PE in negative ion mode, parent-ion scanning of m/z 196; 20-35V, PS in negative ion mode, neutral-loss scanning of m/z 87; and 40-90V, for all glycerophospholipids (including PA, PG and CL) detected by precursor scanning for *m/z* 153 in negative ion mode. MS-MS daughter ion scanning was performed with collision energies between 35-90V. Assignment of phospholipid species was based upon a combination of survey, daughter, precursor and neutral loss scans, as well as previous assignments[76]. The identity of phospholipid peaks was verified using the LIPID MAPS: Nature Lipidomics Gateway (www.lipidmaps.org).

Thin-layer chromatography of lipid extracts: For quantitation, lipid was extracted from purified MscS according to the method of Bligh and Dyer[75]. Briefly, purified MscS was mixed with chloroform:methanol (1:2, 375 μL) v/v for 5 min. Chloroform (125 μl) was added and mixed, followed by the addition of 1 M KCl (125 μL). After vortexing for 1 min, the mixture was centrifuged at 310g for 5 min. The lower phase containing lipids was dried under a nitrogen stream and dissolved in methanol (50 μL). The extracted lipids were spotted on SILICA 60 plates (Macherey-Nagel) and separated in a TLC tank pre-saturated with chloroform:methanol:1M KCl (10:10:3) v/v/v. The plate was air-dried and then stained with 0.05% primuline in acetone:water (80:20 v/v) to visualize lipids. Spots (lipid/detergent) were viewed with a UV transluminator. Plates were then tested specifically for PE by staining in 0.1% ninhydrin in acetone:water (80:20 v/v) followed by heating until pink PE spots developed. The molar ratio of PE:MscS was determined by densitometric analysis of the lipid spots using the software Bio-rad Image Lab Software and compared with that of known POPE standards.

MD simulations

CG–MD Simulations: Protein structures were converted to a coarse-grained (CG) representation using MARTINI v2.1[77]. During the CG simulations an elastic network model was applied to the protein Cα atoms[78] using a distance cutoff of 7 Å and a force constant of 10 kJ mol^{-1} $Å^{-2}$. Simulations were performed using Gromacs v4.5.5[79] (www.gromacs.org). Self-assembly simulations (50 ns) were used to produce five replicates of a 4:1 POPE:POPG lipid bilayer. Each PE:PG bilayer was aligned with the transmembrane (TM) domain of the protein, and lipids overlapping the protein were removed. The system was solvated by approximately 18,000 water particles, charge neutralized, and the ionic concentration set to ~0.15 M NaCl. Each of the five CG-MD simulations was run for 1 μs.

CG to Atomistic Conversion and Equilibration: The final coordinate sets from the CG simulations systems were converted to atomistic representations using a published protocol[80], yielding a system of ~300,000 atoms. Atomistic MD simulations were performed using the GROMOS96[81] 53a6 force field and the SPC water model[82]. Simulations employed

semi-isotropic pressure coupling with the Parrinello–Rahman barostat[83] and the Berendsen thermostat[84] at 310 K. The LINCS algorithm was used to constrain bond lengths[85]. Long-range electrostatic interactions were modelled using the particle mesh Ewald method[86] and a cutoff of 10 Å was used for van der Waals interactions. Each atomistic system was simulated for 100 ns. Visualization used in-built and custom scripted features for VMD 1.9.1[68].

Analysis: To allow a degree of equilibration of protein–lipid interactions, only the latter half of each simulation trajectory was analyzed, i.e. from 0.5 to 1 μs of the CG and from 50 to 100 ns of the AT-MD simulations. The analysis of lipid contacts with MscS used a sampling time of 0.25 ns for AT and 2.5 ns for CG simulations. Contacts were assessed for the full TM domain (residues 27 to 128) and for the lower part of the pocket (TM helix 3, residues 106 to 122). Lipid metrics per residue were averaged across all 7 polypeptide chains and time in a given trajectory. Significant differences between states were calculated using the two-tailed Student's t-test, employing the null hypothesis of no difference and rejecting this when $p \leq 0.01$.

Single-channel planar lipid bilayer recordings—Planar lipid bilayer recordings of single MscS channels were carried out by using bilayers of 1, 2-diphytanoyl-sn-glycero-3-phosphocholine (DPhPC, Avanti Polar Lipids) formed across an aperture (~70 μm in diameter) in a 25-μm thick polytetrafluoroethylene (Teflon) film (Goodfellow, Cambridge), which separated the apparatus into *cis* and *trans* compartments[87]. Bilayers were formed by first pre-treating the aperture with hexadecane in n-pentane (1 μl, 10 mg mL^{-1}) on each side. Both compartments were then filled with the electrolyte solution (200 mM KCl, 90 mM $MgCl_2$, 10 mM $CaCl_2$, 10 mM HEPES, pH 7.5) and DPhPC in n-pentane (5 μl, 5 mg mL^{-1}) was added to both sides to allow membrane formation when the electrolyte was raised above the aperture. The MscS channel was reconstituted by adding 1 μL of a 50 μg mL^{-1} of solution of MscS in 0.05 % DDM, to the *cis* compartment of a planar bilayer apparatus containing 1 mL of electrolyte. This brought the detergent concentration below the CMC causing protein aggregation and precipitation; at the same time, a few channels spontaneously inserted into the lipid bilayer. Fifteen minutes after the addition, assuming that one or a few channels had spontaneously inserted into the lipid bilayer, LPC was added to the *cis* or the *trans* compartment for channel activation, which was manifested by a jump in the ionic current (from 0 pA). We used LPC 14:0 (CMC 43 μM at room temperature[88]), LPC 18:1 and (LPC 18:0 at RT is 0.4 μM at room temperature[88]). Two independent preparations of DDM-purified WT MscS were used for the planar lipid bilayer recordings. Electrical currents were measured with two Ag/AgCl electrodes that were connected to the headstage of a patch-clamp amplifier (Axopatch 200B, Molecular Devices) operating in voltage-clamp mode. The *cis* compartment was connected to the grounded electrode and the *trans* compartment was connected to the working electrode. The data were filtered by an analogue low-pass 4-pole Bessel filter at 2 kHz, and digitally sampled at 10 kHz (Digidata 1440A digitizer, Molecular Devices). The data were analyzed and prepared for presentation with pClamp (version 10.2, Molecular Devices). In control experiments, LPC 14:0 and 18:1 were added to lipid bilayers at different concentrations and bilayers were stable to LPC however, higher concentrations resulted in bilayer rupture.

Supplementary Material

Refer to Web version on PubMed Central for supplementary material.

Acknowledgements

This work was supported by Wellcome Trust Grants WT092552MA (JHN, IRB), Senior Investigator Award WT100209MA (JHN), 093228 (TKS), 092970 (MSPS) and BBSRC grants BB/I019855/1 (MPS), BB/H017917/1 (JHN, IRB), BB/J009784/1 (HB). We acknowledge Diamond Light Source for beam time. IRB is supported as Leverhulme Emeritus Fellow. JHN is a Royal Society Wolfson Merit Award holder and 1000 talent scholar at Sichuan. ACED was supported by an Engineering and Physical Sciences Research Council Systems Biology Doctoral Training Centre student fellowship. We thank R. Phillips, A. Lee and S. Conway for helpful discussions.

References

1. Pivetti CD, et al. Two families of mechanosensitive channel proteins. Microbiol Mol Biol Rev. 2003; 67:66–85. [PubMed: 12626684]
2. Kung C. A possible unifying principle for mechanosensation. Nature. 2005; 436:647–654. [PubMed: 16079835]
3. Arnadottir J, Chalfie M. Eukaryotic mechanosensitive channels. Annu Rev Biophys. 2010; 39:111–137. [PubMed: 20192782]
4. Volkers L, Mechioukhi Y, Coste B. Piezo channels: from structure to function. Pflugers Arch. 2015; 467:95–99. [PubMed: 25037583]
5. Naismith JH, Booth IR. Bacterial mechanosensitive channels--MscS: evolution's solution to creating sensitivity in function. Annu Rev Biophys. 2012; 41:157–177. [PubMed: 22404681]
6. Haswell ES, Phillips R, Rees DC. Mechanosensitive channels: what can they do and how do they do it? Structure. 2011; 19:1356–1369. [PubMed: 22000509]
7. Martinac B. Bacterial mechanosensitive channels as a paradigm for mechanosensory transduction. Cell Physiol Biochem. 2011; 28:1051–1060. [PubMed: 22178995]
8. Levina N, et al. Protection of Escherichia coli cells against extreme turgor by activation of MscS and MscL mechanosensitive channels: identification of genes required for MscS activity. Embo Journal. 1999; 18:1730–1737. [PubMed: 10202137]
9. Reuter M, et al. Mechanosensitive channels and bacterial cell wall integrity: does life end with a bang or a whimper? J R Soc Interface. 2014; 11:20130850. [PubMed: 24258154]
10. Booth IR. Bacterial mechanosensitive channels: progress towards an understanding of their roles in cell physiology. Curr Opin Microbiol. 2014; 18:16–22. [PubMed: 24607989]
11. Shapovalov G, Lester HA. Gating transitions in bacterial ion channels measured at 3 microns resolution. J. Gen. Physiol. 2004; 124:151–161. [PubMed: 15277576]
12. Edwards MD, et al. Pivotal role of the glycine-rich TM3 helix in gating the MscS mechanosensitive channel. Nature Structural & Molecular Biology. 2005; 12:113–119.
13. Anishkin A, Sukharev S. State-stabilizing Interactions in Bacterial Mechanosensitive Channel Gating and Adaptation. J. Biol. Chem. 2009; 284:19153–19157. [PubMed: 19383606]
14. Cox CD, et al. Selectivity mechanism of the mechanosensitive channel MscS revealed by probing channel subconducting states. Nat Commun. 2013; 4:2137. [PubMed: 23842527]
15. Perozo E, Cortes DM, Sompornpisut P, Kloda A, Martinac B. Open channel structure of MscL and the gating mechanism of mechanosensitive channels. Nature. 2002; 418:942–948. [PubMed: 12198539]
16. Vasquez V, Sotomayor M, Cordero-Morales J, Schulten K, Perozo E. A structural mechanism for MscS gating in lipid bilayers. Science. 2008; 321:1210–1214. [PubMed: 18755978]
17. Sukharev SI, Martinac B, Arshavsky VY, Kung C. Two types of mechanosensitive channels in the Escherichia coli cell envelope: solubilization and functional reconstitution. Biophys. J. 1993; 65:177–183. [PubMed: 7690260]
18. Kung C, Martinac B, Sukharev S. Mechanosensitive channels in microbes. Annu. Rev. Microbiol. 2010; 64:313–329. [PubMed: 20825352]

19. Wang W, et al. The structure of an open form of an E. coli mechanosensitive channel at 3.45 A resolution. Science. 2008; 321:1179–1183. [PubMed: 18755969]
20. Bass RB, Strop P, Barclay M, Rees DC. Crystal structure of Escherichia coli MscS, a voltage-modulated and mechanosensitive channel. Science. 2002; 298:1582–1587. [PubMed: 12446901]
21. Anishkin A, Sukharev S. Water dynamics and dewetting transitions in the small mechanosensitive channel MscS. Biophys. J. 2004; 86:2883–2895. [PubMed: 15111405]
22. Akitake B, Anishkin A, Liu N, Sukharev S. Straightening and sequential buckling of the pore-lining helices define the gating cycle of MscS. Nature Structural & Molecular Biology. 2007; 14:1141–1149.
23. Pliotas C, et al. Conformational state of the MscS mechanosensitive channel in solution revealed by pulsed electron-electron double resonance (PELDOR) spectroscopy. Proc. Natl. Acad. Sci. U S A. 2012; 109:E2675–82. [PubMed: 23012406]
24. Ward R, et al. Probing the structure of the mechanosensitive channel of small conductance in lipid bilayers with pulsed electron-electron double resonance. Biophys. J. 2014; 106:834–842. [PubMed: 24559986]
25. Lai JY, Poon YS, Kaiser JT, Rees DC. Open and shut: crystal structures of the dodecylmaltoside solubilized mechanosensitive channel of small conductance from Escherichia coli and Helicobacter pylori at 4.4 A and 4.1 A resolutions. Protein Sci. 2013; 22:502–509. [PubMed: 23339071]
26. Zhang X, et al. Structure and molecular mechanism of an anion-selective mechanosensitive channel of small conductance. Proc. Natl. Acad. Sci. U S A. 2012; 109:18180–18185. [PubMed: 23074248]
27. Brohawn SG, del Marmol J, MacKinnon R. Crystal structure of the human K2P TRAAK, a lipid- and mechano-sensitive K+ ion channel. Science. 2012; 335:436–441. [PubMed: 22282805]
28. Miller AN, Long SB. Crystal structure of the human two-pore domain potassium channel K2P1. Science. 2012; 335:432–436. [PubMed: 22282804]
29. Perozo E, Rees DC. Structure and mechanism in prokaryotic mechanosensitive channels. Curr. Opin. Struct. Biol. 2003; 13:432–442. [PubMed: 12948773]
30. Moe P, Blount P. Assessment of potential stimuli for mechano-dependent gating of MscL: effects of pressure, tension, and lipid headgroups. Biochemistry. 2005; 44:12239–12244. [PubMed: 16142922]
31. Schmidt D, del Marmol J, MacKinnon R. Mechanistic basis for low threshold mechanosensitivity in voltage-dependent K+ channels. Proc. Natl. Acad. Sci. U S A. 2012; 109:10352–10357. [PubMed: 22675122]
32. Brohawn SG, Su Z, Mackinnon R. Mechanosensitivity is mediated directly by the lipid membrane in TRAAK and TREK1 K+ channels. Proc. Natl. Acad. Sci. U S A. 2014
33. Anishkin A, Kung C. Stiffened lipid platforms at molecular force foci. Proc. Natl. Acad. Sci. U S A. 2013; 110:4886–4892. [PubMed: 23476066]
34. Teng J, Loukin S, Anishkin A, Kung C. The force-from-lipid (FFL) principle of mechanosensitivity, at large and in elements. Pflugers Arch. 2015; 467:27–37. [PubMed: 24888690]
35. Sukharev SI, Sigurdson WJ, Kung C, Sachs F. Energetic and spatial parameters for gating of the bacterial large conductance mechanosensitive channel, MscL. J. Gen. Physiol. 1999; 113:525–539. [PubMed: 10102934]
36. Sukharev S. Purification of the small mechanosensitive channel of Escherichia coli (MscS): the subunit structure, conduction, and gating characteristics in liposomes. Biophys. J. 2002; 83:290–298. [PubMed: 12080120]
37. Brohawn SG, Campbell EB, MacKinnon R. Physical mechanism for gating and mechanosensitivity of the human TRAAK K+ channel. Nature. 2014; 516:126–130. [PubMed: 25471887]
38. Branigan E, Pliotas C, Hagelueken G, Naismith JH. Quantification of free cysteines in membrane and soluble proteins using a fluorescent dye and thermal unfolding. Nat Protoc. 2013; 8:2090–2097. [PubMed: 24091556]
39. Palsdottir H, Hunte C. Lipids in membrane protein structures. Biochim. Biophys. Acta. 2004; 1666:2–18. [PubMed: 15519305]

40. Laganowsky A, et al. Membrane proteins bind lipids selectively to modulate their structure and function. Nature. 2014; 510:172–175. [PubMed: 24899312]
41. Oursel D, et al. Lipid composition of membranes of Escherichia coli by liquid chromatography/tandem mass spectrometry using negative electrospray ionization. Rapid Commun Mass Spectrom. 2007; 21:1721–1728. [PubMed: 17477452]
42. Rasmussen T, et al. Tryptophan in the pore of the mechanosensitive channel MscS: assessment of pore conformations by fluorescence spectroscopy. J. Biol. Chem. 2010; 285:5377–5384. [PubMed: 20037156]
43. Phillips R, Ursell T, Wiggins P, Sens P. Emerging roles for lipids in shaping membrane-protein function. Nature. 2009; 459:379–385. [PubMed: 19458714]
44. Sotomayor M, Schulten K. Molecular dynamics study of gating in the mechanosensitive channel of small conductance MscS. Biophys. J. 2004; 87:3050–3065. [PubMed: 15339798]
45. Rasmussen A, et al. The role of tryptophan residues in the function and stability of the mechanosensitive channel MscS from Escherichia coli. Biochemistry. 2007; 46:10899–10908. [PubMed: 17718516]
46. Carney J, et al. Fluorescence quenching methods to study lipid-protein interactions. Curr Protoc Protein Sci. 2006 **Chapter 19**, Unit 19.12.
47. Racker E, Chien TF, Kandrach A. A cholate-dilution procedure for the reconstitution of the Ca++ pump, 32Pi--ATP exchange, and oxidative phosphorylation. FEBS Lett. 1975; 57:14–18. [PubMed: 1175773]
48. Wiener MC, White SH. Transbilayer distribution of bromine in fluid bilayers containing a specifically brominated analogue of dioleoylphosphatidylcholine. Biochemistry. 1991; 30:6997–7008. [PubMed: 2069956]
49. Knol J, Sjollema K, Poolman B. Detergent-mediated reconstitution of membrane proteins. Biochemistry. 1998; 37:16410–16415. [PubMed: 9819233]
50. Nomura T, et al. Differential effects of lipids and lyso-lipids on the mechanosensitivity of the mechanosensitive channels MscL and MscS. Proc. Natl. Acad. Sci. U S A. 2012; 109:8770–8775. [PubMed: 22586095]
51. Anishkin A, Kamaraju K, Sukharev S. Mechanosensitive channel MscS in the open state: modeling of the transition, explicit simulations, and experimental measurements of conductance. J. Gen. Physiol. 2008; 132:67–83. [PubMed: 18591417]
52. Martinac B, Buechner M, Delcour AH, Adler J, Kung C. Pressure-sensitive ion channel in Escherichia coli. Proc. Natl. Acad. Sci. U S A. 1987; 84:2297–2301. [PubMed: 2436228]
53. Batiza AF, Kuo MM, Yoshimura K, Kung C. Gating the bacterial mechanosensitive channel MscL invivo. Proc. Natl. Acad. Sci. U S A. 2002; 99:5643–5648. [PubMed: 11960017]
54. Marsh D, Horvath LI. Structure, dynamics and composition of the lipid-protein interface. Perspectives from spin-labelling. Biochim. Biophys. Acta. 1998; 1376:267–296. [PubMed: 9804973]
55. Gullingsrud J, Schulten K. Lipid bilayer pressure profiles and mechanosensitive channel gating. Biophys. J. 2004; 86:3496–3509. [PubMed: 15189849]
56. Lee AG. Biological membranes: the importance of molecular detail. Trends Biochem. Sci. 2011; 36:493–500. [PubMed: 21855348]
57. Iscla I, Blount P. Sensing and responding to membrane tension: the bacterial MscL channel as a model system. Biophys. J. 2012; 103:169–174. [PubMed: 22853893]
58. Perozo E, Kloda A, Cortes DM, Martinac B. Physical principles underlying the transduction of bilayer deformation forces during mechanosensitive channel gating. Nat. Struct. Biol. 2002; 9:696–703. [PubMed: 12172537]
59. Tanaka K, Caaveiro JM, Morante K, Gonzalez-Manas JM, Tsumoto K. Structural basis for self-assembly of a cytolytic pore lined by protein and lipid. Nat Commun. 2015; 6:6337. [PubMed: 25716479]
60. Anishkin A, Loukin SH, Teng J, Kung C. Feeling the hidden mechanical forces in lipid bilayer is an original sense. Proc. Natl. Acad. Sci. U S A. 2014; 111:7898–7905. [PubMed: 24850861]
61. Leslie AGW. Recent changes to the MOSFLM package for processing film and image plate data. Joint CCP4 and ESF-EAMCB newsletter on protein crystallography. 1992; (No 26):1–10.

62. CCP4. The CCP4 suite: Programs for Protein Crystallography. Acta Crystallographica Section D. 1994; 50:760–763.
63. Diederichs K, Karplus PA. Better models by discarding data? Acta Crystallogr D Biol Crystallogr. 2013; 69:1215–1222. [PubMed: 23793147]
64. Karplus PA, Diederichs K. Linking crystallographic model and data quality. Science. 2012; 336:1030–1033. [PubMed: 22628654]
65. Joosten RP, Long F, Murshudov GN, Perrakis A. The PDB_REDO server for macromolecular structure model optimization. IUCrJ. 2014; 1:213–220.
66. Binkowski TA, Naghibzadeh S, Liang J. CASTp: Computed atlas of surface topography of proteins. Nucleic Acids Res. 2003; 31:3352–3355. [PubMed: 12824325]
67. Pellegrini-Calace M, Maiwald T, Thornton JM. PoreWalker: a novel tool for the identification and characterization of channels in transmembrane proteins from their three-dimensional structure. PLoS Comput. Biol. 2009; 5:e1000440. [PubMed: 19609355]
68. Humphrey W, Dalke A, Schulten K. VMD: visual molecular dynamics. Journal of molecular graphics. 1996; 14:33–38. [PubMed: 8744570]
69. Booth IR, et al. Physiological analysis of bacterial mechanosensitive channels. Methods Enzymol. 2007; 428:47–61. [PubMed: 17875411]
70. Ladokhin AS, Jayasinghe S, White SH. How to measure and analyze tryptophan fluorescence in membranes properly, and why bother? Anal. Biochem. 2000; 285:235–245. [PubMed: 11017708]
71. Schumann U, et al. YbdG in Escherichia coli is a threshold-setting mechanosensitive channel with MscM activity. Proc. Natl. Acad. Sci. U S A. 2010; 107:12664–12669. [PubMed: 20616037]
72. Sobott F, Hernandez H, McCammon MG, Tito MA, Robinson CV. A tandem mass spectrometer for improved transmission and analysis of large macromolecular assemblies. Anal. Chem. 2002; 74:1402–1407. [PubMed: 11922310]
73. Hernandez H, Robinson CV. Determining the stoichiometry and interactions of macromolecular assemblies from mass spectrometry. Nat Protoc. 2007; 2:715–726. [PubMed: 17406634]
74. Fyffe SA, et al. Reevaluation of the PPAR-beta/delta ligand binding domain model reveals why it exhibits the activated form. Mol. Cell. 2006; 21:1–2. [PubMed: 16387648]
75. BLIGH EG, DYER WJ. A rapid method of total lipid extraction and purification. Can J Biochem Physiol. 1959; 37:911–917. [PubMed: 13671378]
76. Richmond GS, et al. Lipidomic analysis of bloodstream and procyclic form Trypanosoma brucei. Parasitology. 2010; 137:1357–1392. [PubMed: 20602846]
77. Monticelli L, et al. The MARTINI coarse-grained force field: extension to proteins. Journal of Chemical Theory and Computation. 2008; 4:819–834. [PubMed: 26621095]
78. Scott KA, et al. Coarse-grained MD simulations of membrane protein-bilayer self-assembly. Structure. 2008; 16:621–630. [PubMed: 18400182]
79. Hess B, Kutzner C, van der Spoel D, Lindahl E. Gromacs 4, load-balanced, and scalable molecular simulation: algorithms for highly efficient. J. Chem. Theory Comput. 2008; 4:435–447. [PubMed: 26620784]
80. Stansfeld PJ, Sansom MSP. From coarse grained to atomistic: a serial multiscale approach to membrane protein simulations. Journal of Chemical Theory and Computation. 2011; 7:1157–1166. [PubMed: 26606363]
81. Scott WRP, et al. The GROMOS biomolecular simulation program package. The Journal of Physical Chemistry A. 1999; 103:3596–3607.
82. Hermans J, Berendsen HJC, Van Gunsteren WF, Postma JPM. A consistent empirical potential for water–protein interactions. Biopolymers. 1984; 23:1513–1518.
83. Parrinello M, Rahman A. Polymorphic transitions in single crystals: A new molecular dynamics method. Journal of Applied physics. 1981; 52:7182.
84. Berendsen HJC, Postma JPM, van Gunsteren WF, DiNola ARHJ, Haak JR. Molecular dynamics with coupling to an external bath. The Journal of chemical physics. 1984; 81:3684.
85. Hess B, Bekker H, Berendsen HJC, Fraaije JGEM. LINCS: a linear constraint solver for molecular simulations. Journal of computational chemistry. 1997; 18:1463–1472.

86. Darden T, York D, Pedersen L. Particle mesh Ewald: An N· log (N) method for Ewald sums in large systems. The Journal of chemical physics. 1993; 98:10089.

87. Montal M, Mueller P. Formation of bimolecular membranes from lipid monolayers and a study of their electrical properties. Proc. Natl. Acad. Sci. U S A. 1972; 69:3561–3566. [PubMed: 4509315]

88. Kramp W, Pieroni G, Pinckard RN, Hanahan DJ. Observations on the critical micellar concentration of 1-O-alkyl-2-acetyl-sn-glycero-3-phosphocholine and a series of its homologs and analogs. Chem Phys Lipids. 1984; 35:49–62. [PubMed: 6744496]

Europe PMC Funders Author Manuscripts

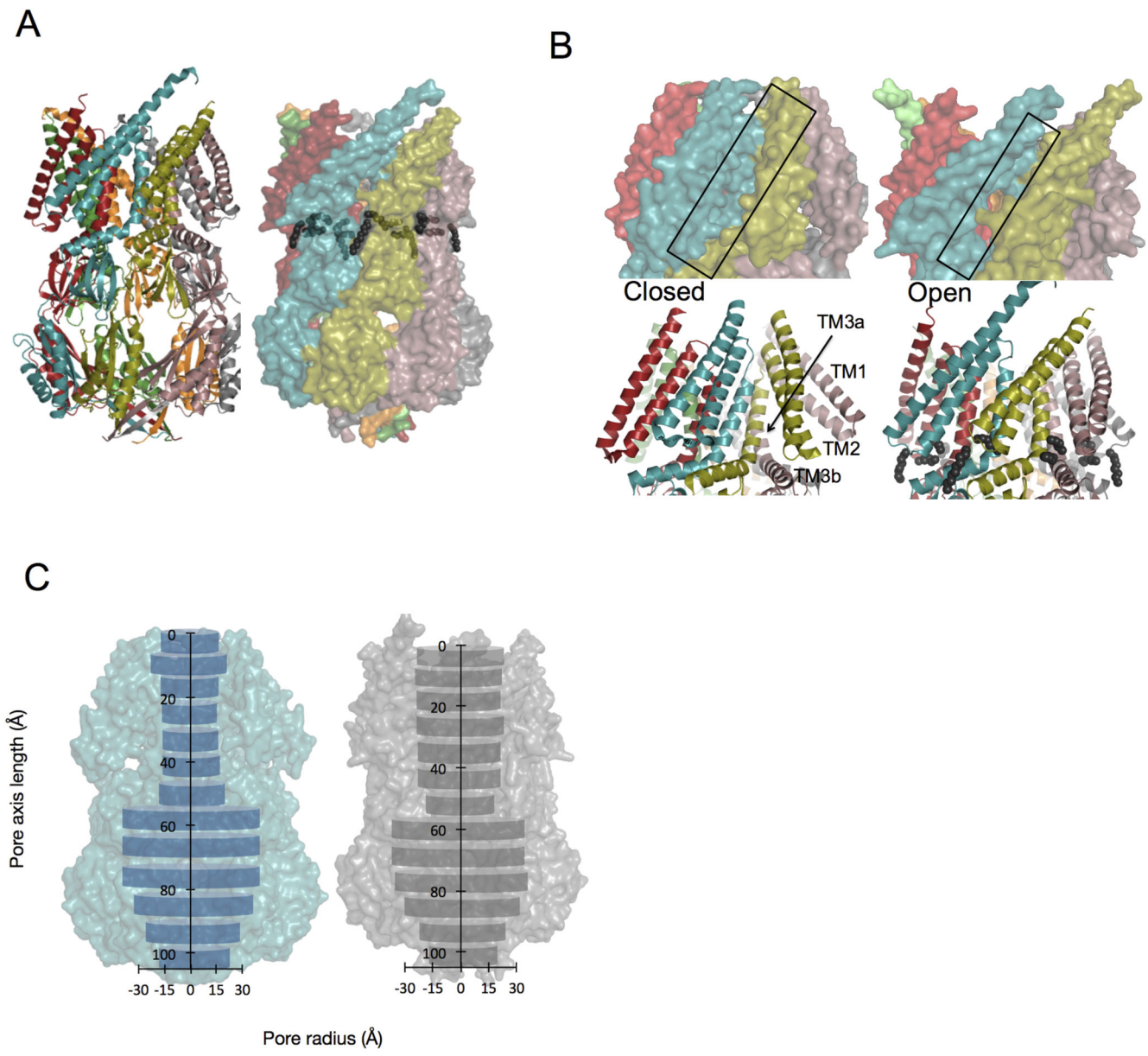

Figure 1. Pockets that are formed between the TM helices that change upon gating

A: The 3.0 Å structure of the D67R1 MscS heptamer shown in cartoon representation on left with a space fill diagram showing the alkyl chains shown on right.

B: The voids between the TM helices undergo large changes upon gating. The pockets (highlighted by black box) in the closed (left) structure[20] are larger than when compared to the open structure (right). The higher resolution of the new structure has allowed to visualize for the first time bound molecules in the pockets (see also Supplementary Fig. 1C).

C: Surface view of the closed (2OAU) and open (D67R1) MscS structures. The open and closed diameters of the pore, which arises from the displacement of the TM3a helices are shown by disks placed along the channel axis.

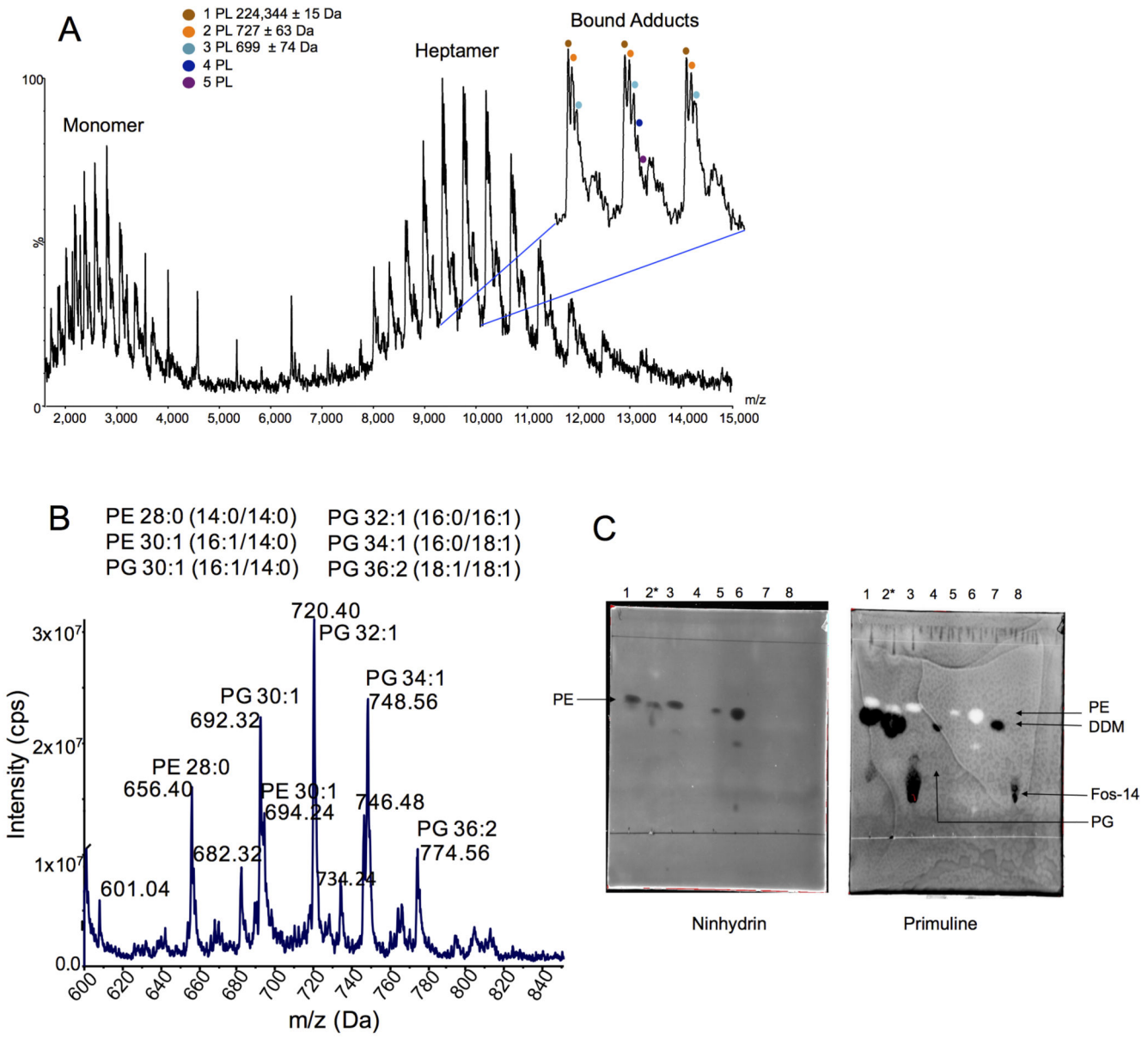

Figure 2. Lipids pack in the pockets created by the TM helices

A: Native mass spectroscopy of wild type MscS, the expected theoretical weight of the heptamer is 223,727 Da. If this value is subtracted from the resolved first peak value of 224,344 Da (brown dot), then it results in around 620Da, consistent with a small lipid (brown dot in Fig 2A). Subsequent differences between peaks reveal additional lipid adducts.

B: ES-MS of phospholipid extracted from a sample of DDM-solubilized MscS.

C: Thin layer chromatogram of extracted lipids from DDM-solubilized MscS. Lipid separation was carried out in the solvent system chloroform:methanol:1M KCl (10:10:3, v/v/v). Spots on the TLC plate were visualized by staining first with a) 0.1% ninhydrin and b) 0.05% primuline, both in acetone:water (80:20, v/v). The samples loaded are Lane [1], MscS-DDM (238 μg)*, [2] MscS-DDM (280 μg), [3] MscS-Fos-14 (305 μg)*, [4] POPG (5

µg), [5] POPE (2.4 µg), [6] *E. coli* lipids (8 µg), [7] DDM (5 µg), [8] Fos-14 (10 µg). The result is typical of three separate experiments. Lanes 1 & 3 were freshly purified, lane 2 was several months old. *mass refers to quantity of MscS protein loaded; others refer to mass of lipids. Note that PG, known to be present from mass spectrometry in preparations 1 & 2, is not visible due to the overlap with the DDM, which is much more abundant in the detergent-solubilized material.

Europe PMC Funders Author Manuscripts

Europe PMC Funders Author Manuscripts

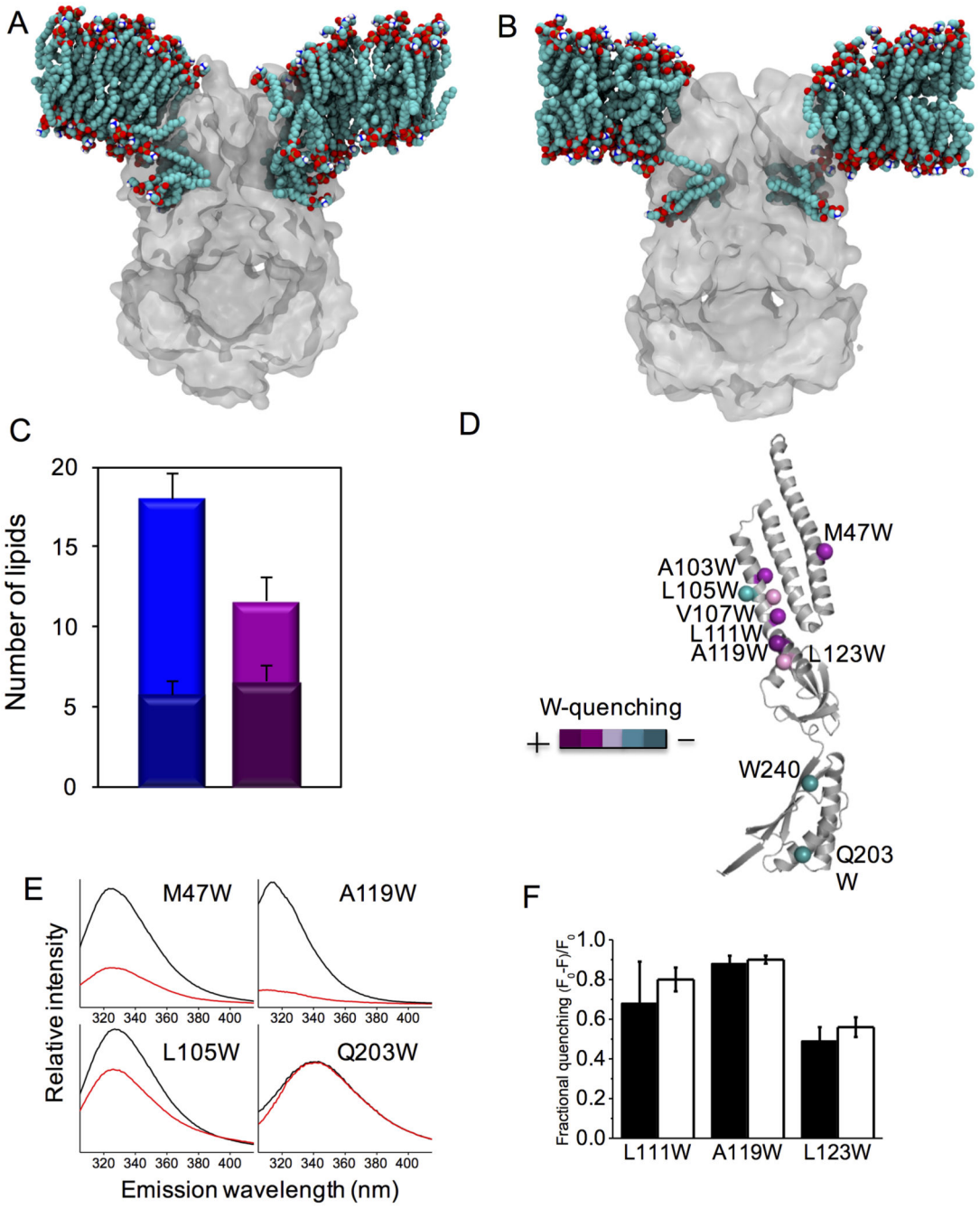

Figure 3. Lipids exchange between the pockets and the bilayer

A cut away slice showing snapshots (at 100 ns) of atomistic simulations of the closed (A) and open (B) conformation of MscS in POPE:POPG (4:1) phospholipid bilayers. Movies of the lipid bilayer (with protein removed) are available as Supplementary files (movie 1 and movie 2).

C: Comparison of the number of lipids that remain within 6 Å of the TM (i.e. residues 27 to 128, light bars) and the lower pocket (TM3b region, residues 106 to 122 (darker shaded bars) of closed (blue bars) and open state (magenta bars) MscS throughout the latter 0.5 μs

of the CG-MD simulations. Error bars indicate one standard deviation of number of lipid contacts. A larger number of lipids are in rapid exchange between the pockets and bilayer (Supplementary Fig. 3E).

D: Single-tryptophan mutants of MscS probed with brominated phospholipids and the degree of quenching is shown by color shading.

E: Typical raw data of quenching experiments (selected mutants). Emission spectra are shown from MscS in 100% DOPC (black) or 100% BrPC (red).

F: Quantitative results of BrPC quenching in form of the fractional quenching by brominated lipid for TM3b mutants in DOPC (black bars; s.d. shown as error bar from n= 17 reconstitutions) and 80% DOPE:20% DOPG (white bars; s.d. shown as error bar from n = 4 reconstitutions)).

Europe PMC Funders Author Manuscripts

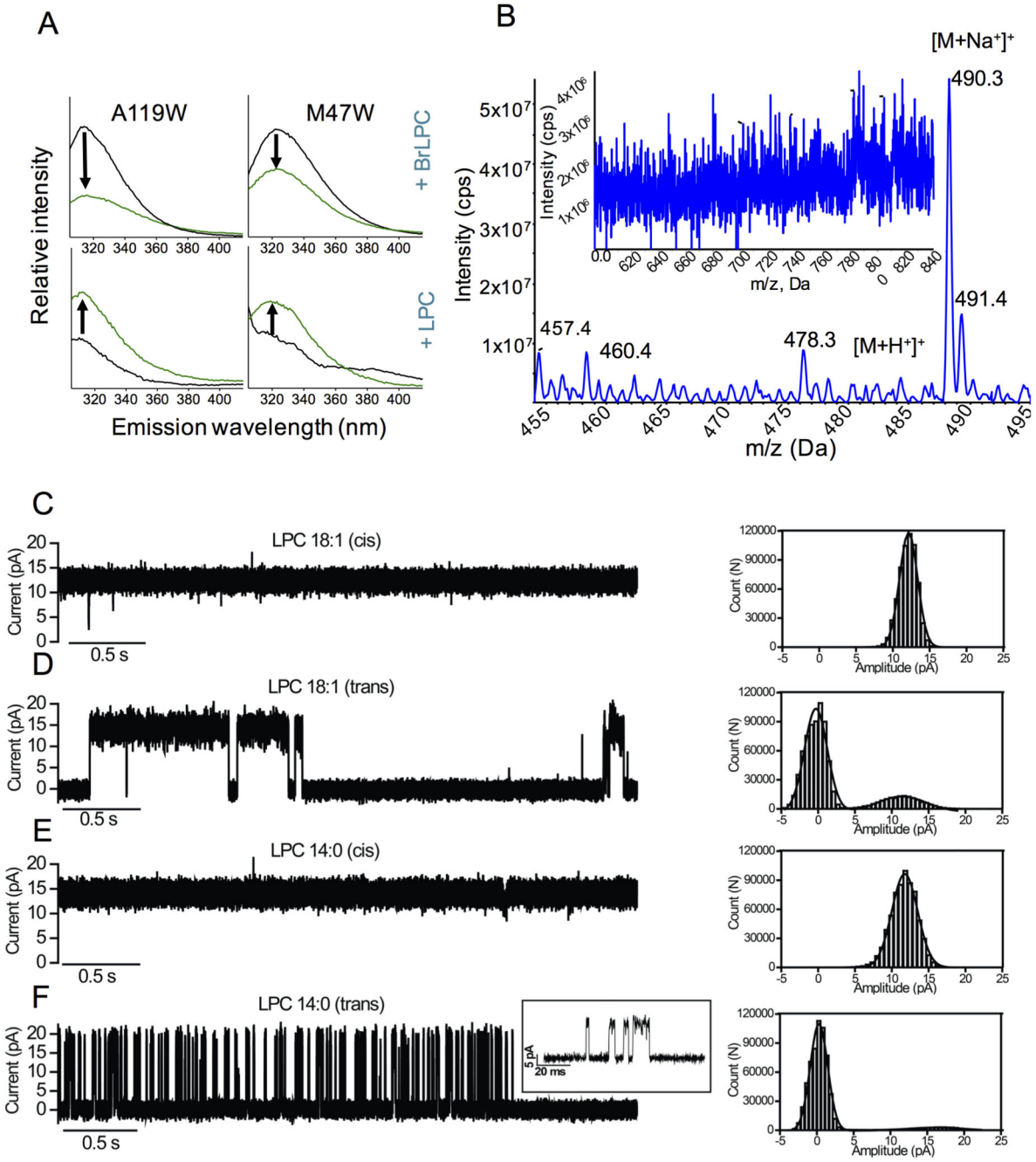

Figure 4. MscS conformational state can be altered by perturbing the interactions between the phospholipid and the protein

A: A119W (left) and M47W (right) were reconstituted into DOPC (top row) or BrPC (bottom row) shown in black. Brominated LPC (top) or non-brominated LPC (bottom) was added (green) causing quenching or dequenching, respectively.

B: ES-MS of phospholipid extracted from DDM-solubilised MscS after treatment with LPC 14:0. Survey scan in positive ion mode (465-500 m/z) showing the 490 m/z of the LPC 14:0. Survey scan in negative ion mode (600-1000 m/z) of MscS after treatment with LPC 14:0 (inset). Only LPC 14:0 [M+Na^+] 490.3 was observed.

C: Typical current recordings of single MscS channels in planar lipid bilayers. The applied potential was at +20 mV. Right panels: corresponding all-points amplitude histograms. In this experiment 3 μM LPC 18:1, was added to the *cis* compartment.
D: As 4C but with 3 μM LPC 18:1 added to the *trans* compartment.
E: As 4C but with 10 μM LPC 14:0 added to the *cis* compartment.
F: As 4C but with 10 μM LPC 14:0, added to the *trans* compartment. Inset: recording at expanded time scale.

Europe PMC Funders Author Manuscripts

Europe PMC Funders Author Manuscripts

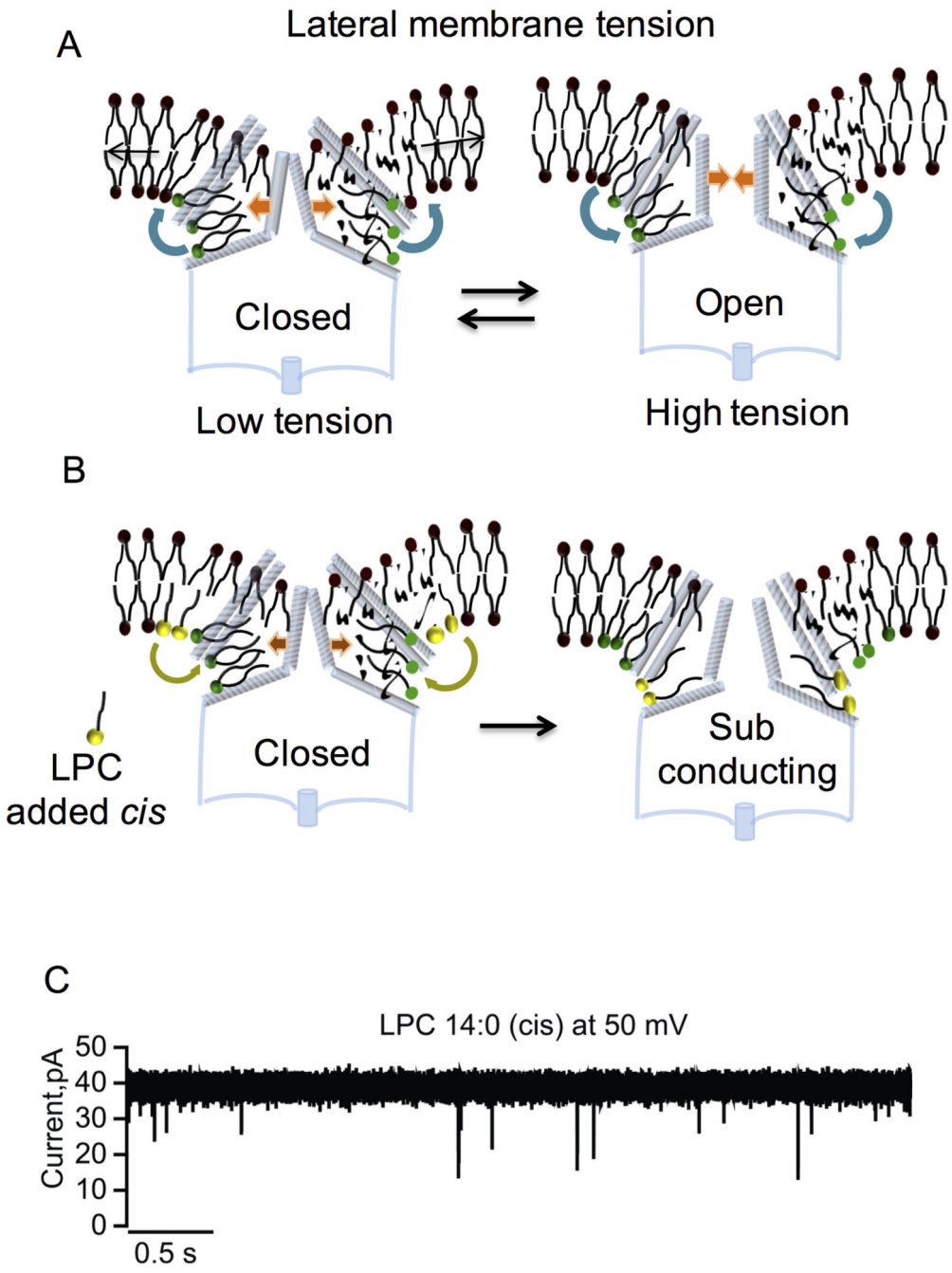

Figure 5. A model for mechanosensation

A: MscS is depicted as a simplified a line diagram, PE and PG molecules are shown with black headgroups, those inside the pockets are highlighted (for easy visualization) with a green headgroup. The phospholipids partition in the pockets and the lipid bilayer. As pressure is applied, the lateral tension increases and as a result the phospholipids repartition (blue arrows) from the protein pockets to the bilayer destabilizing the closed structure. The protein responds by undergoing a conformational change (orange arrow) to the open form.

B: LPC (shown as a single chain with a yellow headgroup) enters first the bilayer then the pockets from the cytoplasmic side and as result the lipid content (acyl chains) falls inside the protein pockets destabilizing the closed structure. The protein undergoes a conformational change to a sub conducting state.

C: Single channel bilayer recordings show that MscS D67C exhibits similar conductivity as WT protein when opened by addition of LPC 14:0 to the *cis* side (Fig 4E).

Europe PMC Funders Author Manuscripts

Europe PMC Funders Author Manuscripts

Table 1

	MscS D67R1
Data collection	
Space group	$P2_12_12_1$
Cell dimensions	
a, b, c (Å)	126.5, 149.0, 174.0
α, β, γ (°)	90, 90, 90
Resolution (Å)	64.2 – 2.99 (3.07 – 2.99)[a]
R_{merge}	0.082 (1.002)
$I / \sigma I$	6.7 (1.1)
Completeness (%)	99.5 (99.8)
Redundancy	3.5 (3.6)
Refinement	
Resolution (Å)	64.2 – 2.99
No. reflections	66747
R_{work} / R_{free}	24.4 / 26.3
No. atoms	
Protein	13733
Ligand	203
Water	
B factors	
Protein	114
Ligand	103
Water	
r.m.s. deviations	
Bond lengths (Å)	0.008
Bond angles (°)	1.2

Data collected on 1 crystal.

[a]Values in parentheses are for highest-resolution shell.